*Inorg. Chem.* **2008**, *47*, 2634−2640

# Evolution of the Crystal Structure of $RVO_3$ (R = La, Ce, Pr, Nd, Tb, Ho, Er, Tm, Yb, Lu, Y) Perovskites from Neutron Powder Diffraction Data

**M. J. Martínez-Lope,[†] J. A. Alonso,[*,†] M. Retuerto,[†] and M. T. Fernández-Díaz[‡]**

*Instituto de Ciencia de Materiales de Madrid, CSIC, Cantoblanco, E-28049 Madrid, Spain, and Institut Laue Langevin, BP 156X, Grenoble F-38042, France*

Received October 5, 2007

$RVO_3$ perovskites have been prepared in the widest range of $R^{3+}$ ionic size, from $LaVO_3$ to $LuVO_3$. Pure polycrystalline samples have been obtained by a citrate technique leading to reactive $RVO_4$ precursors, followed by thermal treatments in a reducing $H_2/N_2$ (15/85%) flow to stabilize $V^{3+}$ cations. These oxides have been studied at room temperature by high-resolution neutron powder diffraction to follow the evolution of the crystal structures along the series. The distortion of the orthorhombic perovskite (space group *Pbnm*), characterized by the tilting angle of the $VO_6$ octahedra, progressively increases from La to Lu due to simple steric factors. Additionally, all of the perovskites show a subtle distortion of the $VO_6$ octahedra which significantly increases from La to Tb, and then slightly decreases for the last terms of the series. The stability of the crystal structure is also discussed in light of bond-valence arguments.

## Introduction

$ABO_3$ oxides with perovskite structure contain infinite, three-dimensional, corner-sharing $BO_6$ octahedra with a dodecahedrally coordinated A-site in the center of a cavity generated by eight surrounding octahedra. The ideal, cubic structure, so-called aristotype, is rarely achieved at ambient temperature because of the strict constraints placed on the A−O and B−O bond lengths, which would be required to be in the exact ratio of $\sqrt{2}$:1, with a tolerance factor ($t$ = A−O/$\sqrt{2}$B−O) equal to unity. In the real world, most perovskites consequently show distortions from the aristotype phase, resulting in what are generally termed hettotype phases. Most frequently, the structural stress is relieved by rotation or tilting of the $BO_6$ octahedra; this is specially suited when the A cation is too small for the dodecahedral site, and allows shortening of A−O bonds, while maintaining the B−O bond lengths. Glazer[1,2] and, more recently, Woodward[3] and Howard and Stokes[4] studied the lowering of symmetry from the aristotype phase in the different systems caused by the tilting of layers of undistorted octahedra around the 4-fold axes of the cubic structure, introducing a convenient notation for the description of the structures derived from these successive tilts. For instance, the most common tilt system is represented by $a^-a^-c^+$,[2] exhibited by the mineral "perovskite" $CaTiO_3$, itself.

Several complete $RMO_3$ perovskite series of rare-earth (R) transition-metal (M) perovskite oxides have been studied in the past (e.g., $RFeO_3$, $RMnO_3$, $RCoO_3$, $RNiO_3$) and they constitute interesting examples were the regular evolution of certain parameters (individual M−O and R−O distances, tilting angle, distortion of the octahedra) can be evaluated as a function of the tolerance factor of the perovskite, progressively changing along the series as the R size becomes smaller due to the lanthanide contraction. For instance, structural data obtained for the $RFeO_3$ perovskite family[5,6] show that the octahedral $FeO_6$ units undergo not only a cooperative rotation, but also an intrinsic site distortion that progressively varies with $R^{3+}$ ionic radius. In the case of the $RMnO_3$ series,[7] the orbital−lattice interaction determining a cooperative Jahn–Teller site distortions are over imposed to the pure tilting effect. Moreover, the orbital-lattice interactions of the 2-fold *e*-orbital degeneracy at the high-

* To whom correspondence should be addressed. E-mail: ja.alonso@icmm.csic.es.
† Instituto de Ciencia de Materiales de Madrid.
‡ Institut Laue Langevin.

(1) Glazer, A. M. *Acta Crystallogr., Sect. B* **1972**, *28*, 3384.
(2) Glazer, A. M. *Acta Crystallogr., Sect. A* **1975**, *31*, 756.
(3) Woodward, P. M. *Acta Crystallogr., Sect. B* **1997**, *53*, 32.
(4) Howard, C. J.; Stokes, H. T. *Acta Crystallogr., Sect. B* **1998**, *54*, 782.
(5) Marezio, M.; Dernier, P. D. *Mater. Res. Bull.* **1971**, *6*, 23.
(6) Marezio, M.; Remeika, J. P.; Dernier, P. D. *Acta Crystallogr., Sect. B* **1971**, *26*, 2008.
(7) Alonso, J. A.; Martínez-Lope, M. J.; Casais, M. T.; Fernández-Díaz, M. T.; *Inorg. Chem.* **2000**, *39*, 917



10.1021/ic701969q CCC: $40.75 
Published on Web 02/27/2008

spin $Mn^{3+}$ ions of the $RMnO_3$ family are much stronger than the spin–spin interactions responsible for the long-range magnetic order, whereas the weaker orbital−lattice interactions of the 3-fold $t_2$ orbital degeneracy at the $Ti^{3+}$ and $V^{3+}$ ions of the $RTiO_3$ and $RVO_3$ families are comparable to the spin–spin interactions, meaning that the spin-ordering temperature is similar to the orbital ordering temperature, and the on-site spin–orbit coupling would compete with the orbital−lattice interactions for determination of the character of the cooperative Jahn–Teller distortion.

Rare-earth orthovanadates with the chemical formula $RVO_3$ form a very interesting system that exhibits outstanding physical properties, as anomalous diamagnetism and an almost simultaneous crystallographic−antiferromagnetic transition, as a consequence of the comparable spin–spin and orbital−lattice interactions. The compounds of this system are semiconducting or insulating, although some of them, like the Mott insulator $YVO_3$ oxide, can become metallic by carrier doping.

The magnetic properties of the rare-earth orthovanadates have been well studied;[8–21] the most singular feature is the presence of the anomalous diamagnetism effect. The origin of the apparent diamagnetism in $LaVO_3$ is a canted-spin antiferromagnetism that orients its magnetization in opposition to the magnetizing field on cooling through an orbital-ordering crystallographic transition temperature $T_{OO1} < T_N$.[22] Below the magnetic-ordering temperature, with $T_N$ ranging from 137 K for $LaVO_3$ to 101 K for $LuVO_3$,[8] the members of the series adopt an antiferromagnetic-canted magnetic structure. When $R^{3+}$ is large and thus the orthorhombic lattice distortion is small, the AF structure is *C*-type with the $V^{3+}$ ($S = 1$) spins antiferromagnetically coupled in the *ab* plane, these AF layers being ferromagnetically arranged along the *c*-axis. On the other hand, for relatively small R-site ions the patterns of the magnetic structure is G-type, with AF coupling of the $V^{3+}$ spins in all three directions.

The first crystallographic studies reported in the fifties described $RVO_3$ from R = Pr to Lu as orthorhombic.[23–25] with $a \approx b \approx \sqrt{2}a_p$ and $b \approx 2a_p$, *Pbnm* space group (the long axis parallel to the *c*-direction), whereas $LaVO_3$ was considered to be cubic with $a \approx 2a_p$, with $a_p$ being the lattice parameter of the ideal cubic perovskite. A subsequent work carried out on $LaVO_3$ showed that this compound is also orthorhombic, isostructural with $GdFeO_3$.[26] A decrease in the orthorhombic unit-cell volume is observed on decreasing the ionic radius of the $R^{3+}$ cation, as expected by the lanthanide contraction effect.

A systematic study of the crystal structure of all the compounds of the series by neutron diffraction is lacking. This technique is specially suitable to study the structure of vanadium perovskites since the almost null scattering factor for V (placed at special positions of the Pbnm space group) boosts the contrast of the oxygen sublattice, allowing a precise determination of the oxygen positions. In this paper, we describe the preparation of the full series of nonabsorbing $RVO_3$ (R = La, Ce, Pr, Nd, Tb, Ho, Er, Tm, Yb, Lu, Y) perovskites performed from room-temperature neutron diffraction data, and discuss on the evolution of different structural parameters across the series. The intermediate $SmVO_3$, $EuVO_3$, $GdVO_3$, and $DyVO_3$ have been excluded from this study given the large neutron absorption cross-section of the corresponding rare earths.

## Experimental Section

$RVO_3$ (R = La, Ce, Pr, Nd, Tb, Ho, Er, Tm, Yb, Lu, Y) perovskites were prepared in polycrystalline form from citrate precursors obtained by soft-chemistry procedures. Stoichiometric amounts of analytical grade $R_2O_3$ and $NH_4VO_3$ were dissolved in citric acid by adding several drops of concentrated $HNO_3$ to favor the solution of rare-earth oxides. The citrate + nitrate solutions were slowly evaporated, leading to organic resins containing a random distribution of the involved cations at an atomic level. These resins were first dried at 120 °C and then slowly decomposed at temperatures up to 600 °C. All the organic materials and nitrates were eliminated in a subsequent treatment at 800 °C in air for 2 h. This treatment gave rise to $RVO_4$ oxides, with zircon structure, conformed as highly reactive precursor materials. The precursors were finally reduced at 1160 °C for 12 h in a $H_2/N_2$ (15%/85%) flow.

The initial characterization of the products was carried out by laboratory X-ray diffraction (XRD) (Cu Kα, $\lambda = 1.5418$ Å). Neutron powder diffraction (NPD) diagrams were collected at the Institut Laue-Langevin (ILL) in Grenoble (France). The crystallographic structures were refined from the high-resolution NPD patterns, acquired at room temperature at the D2B diffractometer with $\lambda = 1.594$ Å. The refinement of the crystal structures was performed by the Rietveld method,[27] using the FULLPROF refinement program.[28] A pseudo-Voigt function was chosen to generate the line shape of the diffraction peaks. As V metal from


(8) Zubkov, V. G.; Bazner, G. V.; Shveitin, G. P. *Sov. Phys. Solid State* **1976**, *18*, 1165.
(9) Bazner, G. V.; Matveenko, J. J.; Shveikin, G. P. *Sov. Phys. Solid State* **1974**, *16*, 155.
(10) Sakai, T.; Adachi, G.; Shiokawa, J.; Shin-ike, T. *Mater. Res. Bull.* **1976**, *11*, 1295.
(11) Rogers, D. B.; Ferretti, A.; Ridgley, D. H.; Arnott, R. J.; Goodenough, J. B. *J. Appl. Phys.* **1966**, *37*, 1431.
(12) Dougier, P.; Hagenmuller, P. *J. Solid State Chem.* **1975**, *15*, 158.
(13) Kimishima, Y.; Takahashi, M.; Iga, K.; Okada, K.; Ichiyanagi, Y. *Physica B* **1994**, *211*, 194–196.
(14) Kimishima, Y.; Takahashi, M.; Okada, K.; Ishikawa, H.; Ichiyanagi, Y. *J. Magn. Magn. Mater.* **1995**, *1185*, 140–144.
(15) Onoda, M.; Nagasawa, H. *Solid State Commun.* **1996**, *99*, 487.
(16) Kimishima, Y.; Ichiyanagi, Y.; Shimizu, K.; Mizuno, T. *J. Magn. Magn. Mater.* **2000**, *210*, 244.
(17) Muñoz, A.; Alonso, J. A.; Casais, M. T.; Martínez-Lope, M. J.; Fernández-Díaz, M. T. *J. Mater. Chem.* **2003**, *13*, 1234.
(18) Nguyen, H. C.; Goodenough, J. B. *Phys. Rev. B* **1995**, *52*, 324.
(19) Nguyen, H. C.; Goodenough, J. B. J. *Solid State Chem.* **1995**, *119*, 24.
(20) Ren, Y.; Palstra, T. T. M.; Khomskii, D. I.; Nugroho, A. A.; Menovsky, A. A.; Sawatzky, G. A. *Nature* **1998**, *396*, 441.
(21) Ren, Y.; Palstra, T. T. M.; Khomskii, D. I.; Nugroho, A. A.; Menovsky, A. A.; Sawatzky, G. A. *Phys. Rev. B* **2000**, *62*, 6577.
(22) Goodenough, J. B.; Nguyen, H. C. *C.R. Acad. Sci.* **1994**, *319*, 1285.
(23) Yakel, H. L. *Acta Crystallogr.* **1955**, *8*, 394.
(24) Bertaut, F.; Forrat, F. *J. Phys. Radium* **1956**, *17*, 129.
(25) Geller, S. *Acta Crystallogr.* **1957**, *10*, 243.
(26) Bordet, P.; Chaillout, C.; Marezio, M.; Huang, Q.; Santoro, A.; Cheong, S-W.; Takagi, H.; Oglesby, C. S.; Batlogg, B. *J. Solid State Chem.* **1993**, *106*, 253.
(27) Rietveld, H. M. *J. Appl. Crystallogr.* **1969**, *2*, 65.
(28) Rodríguez-Carvajal, J. *Physica B* **1993**, *192*, 55.

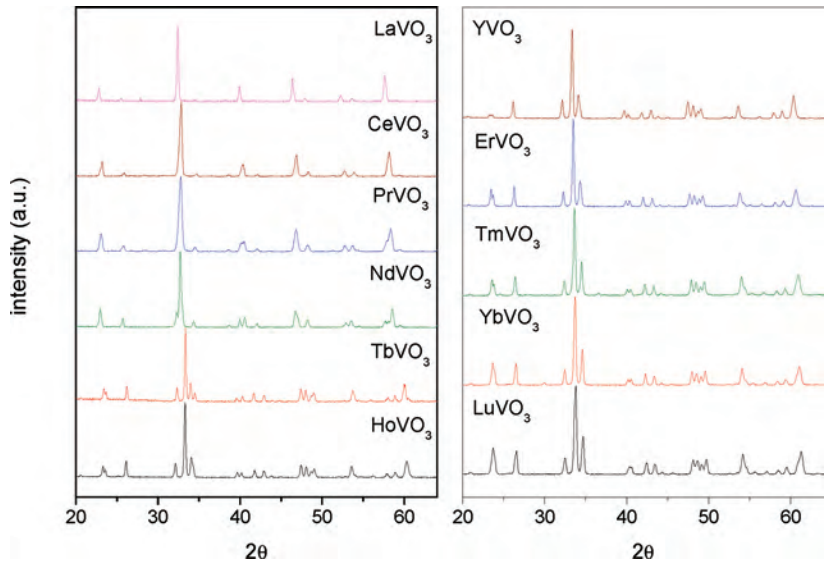


**Figure 1.** Laboratory XRD patterns for $RVO_3$, R = La, Ce, Pr, Nd, Tb, Ho, Y, Er, Tm, Yb, and Lu.

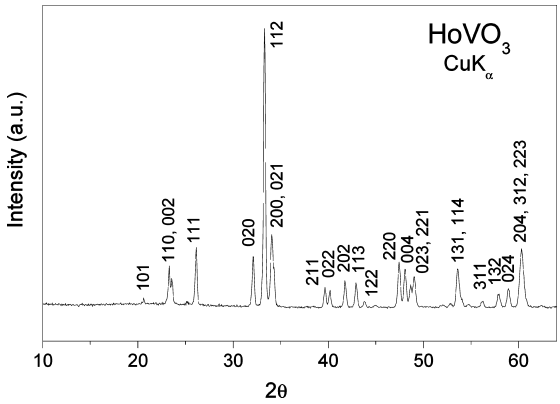


**Figure 2.** $HoVO_3$ XRD pattern indexed in an orthorhombic unit cell with $a = 5.2853(3)$, $b = 5.5953(3)$, $c = 7.5891(4)$ Å.

the sample holder was detected in some diagrams, it was introduced in the refinement as a second phase (space group $Im\bar{3}m$, $a = 3.024$ Å). The following parameters were refined in the final runs: scale factors, background coefficients, zero-point error, pseudo-Voigt corrected for asymmetry parameters, positional coordinates and isotropic thermal factors. The coherent scattering lengths for La, Ce, Pr, Nd, Tb, Ho, Er, Tm, Yb, Lu, Y, V and O were 8.24, 4.84, 4.58, 7.69, 7.38, 8.01, 7.79, 7.07, 12.4, 7.21, 7.75, –0.382, and 5.803 fm, respectively.

## Results and Discussion

Polycrystalline samples of $RVO_3$, R = La, Ce, Pr, Nd, Tb, Ho, Er, Tm, Yb, Lu, and Y have been obtained as black, well-crystallized powders. The laboratory XRD diagrams are shown in Figure 1. The patterns are characteristic of distorted perovskites showing sharp, well-defined superstructure reflections. The XRD diagrams were indexed in the conventional Pbnm orthorhombic model, with unit-cell parameters related to $a_0$ (ideal cubic perovskite, $a_0 \approx 3.8$ Å) as $a \approx \sqrt{2}a_0$, $b \approx \sqrt{2}a_0$, $c \approx 2a_0$; Figure 2 illustrates the indexing of the strongly distorted $HoVO_3$ perovskite. The structural refinement was performed from NPD in the orthorhombic space group *Pbnm* (No.62), $Z = 4$, with the $GdFeO_3$-type structure.[26] R atoms were located at 4*c* positions, V atoms at 4*b*, and oxygen atoms at 4*c* and 8*d* positions, respectively. Because the scattering power of V is very weak, the thermal factor of this atom was fixed to 0.4 Å.[2] The final unit-cell parameters, atomic coordinates, and discrepancy factors after the refinements are given in Tables 1 and 2. Table 3 contains a selected list of distances and angles. Figure 3 illustrates the goodness of the fit for two representative members of the series, $NdVO_3$ and $TbVO_3$. Figure 4 depicts the evolution of the unit-cell dimensions and volume with the ionic $R^{3+}$ size, taken from Shannon[29] for 8-fold coordination. The variation of the *b* parameter is very small compared to that of *a* and *c*; this is due to the tilting scheme of $VO_6$ octahedra in *Pbnm* perovskites, of the type $a^-a^-c^+$ in Glazer's nomenclature,[2] in which the distortion driven by the reduction of the $R^{3+}$ size leaves *b* almost unchanged. The observed decrease in unit-cell volume scales with the $R^{3+}$ size. It is worth mentioning that, in all cases, $c/\sqrt{2}$ lies between *a* and *b*. This is characteristic of the so-called O structure and constitutes the usual situation in perovskites where the primary distorting effect is steric, driven by the reduction in size of $R^{3+}$ cations.

The spontaneous orthorhombic strain, defined as $s = 2(b - a)/(a + b)$, is included in Table 1. *s* progressively increases

**Table 1.** Unit-Cell Parameters and Volume for $RVO_3$ in the Orthorhombic *Pbnm* Space Group from NPD at 295 K [a]

| R | r($R^{3+}$) (Å)[b] | *a* (Å) | *b* (Å) | *c* (Å) | *V* (Å$^3$) | *s* |
|---|---|---|---|---|---|---|
| La | 1.160 | 5.5552(2) | 5.5493(1) | 7.8432(2) | 241.78(1) | −0.0011 |
| Ce | 1.143 | 5.5178(2) | 5.5515(2) | 7.8061(3) | 239.11(2) | 0.0061 |
| Pr | 1.126 | 5.4856(2) | 5.5606(2) | 7.7771(3) | 237.23(2) | 0.0136 |
| Nd | 1.109 | 5.4550(2) | 5.5716(2) | 7.7482(3) | 235.49(2) | 0.0211 |
| Tb | 1.040 | 5.3297(2) | 5.5938(2) | 7.6267(3) | 227.38(1) | 0.0484 |
| Y | 1.019 | 5.2824(2) | 5.5927(2) | 7.5831(3) | 224.02(2) | 0.0571 |
| Ho | 1.015 | 5.2853(3) | 5.5953(3) | 7.5891(4) | 224.43(2) | 0.0569 |
| Er | 1.004 | 5.2644(3) | 5.5856(4) | 7.5716(5) | 222.64(3) | 0.0592 |
| Tm | 0.994 | 5.2453(4) | 5.5761(5) | 7.5551(5) | 220.98(3) | 0.0611 |
| Yb | 0.985 | 5.2320(1) | 5.5662(2) | 7.5446(2) | 219.72(1) | 0.0619 |
| Lu | 0.977 | 5.2156(2) | 5.5611(3) | 7.5347(3) | 218.54(2) | 0.0641 |

[a] The orthorhombic strain is defined as $s = 2(b - a)/(a + b)$. [b] Taken from ref 29.

(29) Shannon, R. D. *Acta Crystallogr., Sect. A* **1976**, *32*, 751.

**Table 2.** Structural Parameters after the Rietveld Refinement of NPD Data for $RVO_3$ at 295 K[a]

| | atom | | | | | | | | | | |
|---|---|---|---|---|---|---|---|---|---|---|---|
| | La | Ce | Pr | Nd | Tb | Y | Ho | Er | Tm | Yb | Lu |
| R | | | | | | | | | | | |
| *x* | 0.9939(5) | 0.9914(13) | 0.9928(7) | 0.9904(4) | 0.9827(3) | 0.9808(3) | 0.9811(4) | 0.9798(5) | 0.9802(6) | 0.97976(17) | 0.9788(3) |
| *y* | 0.0296(2) | 0.0370(8) | 0.0448(5) | 0.0498(3) | 0.0645(2) | 0.0682(3) | 0.0667(4) | 0.0694(4) | 0.0656(6) | 0.07044(15) | 0.0708(3) |
| *B* (Å$^2$) | 0.62(2) | 0.49(6) | 0.65(3) | 0.45(2) | 0.39(2) | 0.42(3) | 0.32(4) | 0.30(4) | 0.46(5) | 0.51(2) | 0.41(3) |
| O1 | | | | | | | | | | | |
| *x* | 0.0733(6) | 0.0765(8) | 0.0818(4) | 0.0861(5) | 0.1037(4) | 0.1109(4) | 0.1108(5) | 0.1124(6) | 0.1120(7) | 0.1176(3) | 0.1198(4) |
| *y* | 0.4890(4) | 0.4842(7) | 0.4809(3) | 0.4790(4) | 0.4655(3) | 0.4605(4) | 0.4604(6) | 0.4596(6) | 0.4522(8) | 0.4556(4) | 0.4544(4) |
| *B* (Å$^2$) | 0.68(3) | 0.77(6) | 0.71(3) | 0.56(4) | 0.62(3) | 0.59(4) | 0.67(6) | 0.57(6) | 1.14(7) | 0.51(3) | 0.51(4) |
| O2 | | | | | | | | | | | |
| *x* | 0.7169(3) | 0.7113(5) | 0.7062(3) | 0.7040(3) | 0.6942(2) | 0.6912(3) | 0.6909(4) | 0.6900(4) | 0.6884(5) | 0.6882(2) | 0.6884(3) |
| *y* | 0.2831(3) | 0.2888(4) | 0.2930(3) | 0.2947(3) | 0.3020(3) | 0.3035(3) | 0.3045(4) | 0.3043(5) | 0.3065(5) | 0.3065(2) | 0.3070(3) |
| *z* | 0.0377(2) | 0.0414(3) | 0.0429(2) | 0.0453(2) | 0.05350(15) | 0.05618(17) | 0.0553(2) | 0.0566(3) | 0.0564(3) | 0.05929(15) | 0.06034(15) |
| *B* (Å$^2$) | 0.71(2) | 0.69(4) | 0.67(2) | 0.61(3) | 0.61(2) | 0.59(3) | 0.65(4) | 0.65(4) | 0.73(4) | 0.65(2) | 0.59(2) |
| $\chi^2$ | 1.59 | 1.00 | 1.20 | 1.28 | 1.18 | 1.16 | 1.17 | 1.02 | 1.51 | 1.37 | 1.08 |
| $R_p$ (%) | 3.57 | 4.21 | 3.31 | 3.37 | 2.96 | 3.64 | 3.36 | 3.03 | 4.22 | 3.14 | 3.40 |
| $R_{wp}$ (%) | 4.66 | 5.22 | 4.23 | 4.23 | 3.69 | 4.54 | 4.20 | 3.76 | 5.38 | 3.99 | 4.26 |
| $R_{exp}$ (%) | 3.69 | 5.21 | 3.86 | 3.74 | 3.40 | 4.22 | 3.87 | 3.72 | 4.38 | 3.41 | 4.09 |
| $R_I$ (%) | 4.00 | 7.34 | 4.06 | 4.31 | 4.81 | 3.86 | 7.32 | 6.50 | 9.61 | 3.50 | 3.77 |

[a] R, O1 at 4*c* (*x*, *y*, 1/4), *V* at 4*b* (1/2,0,0), and O2 at 8*d* (x,y,z) positions.

from R = La to R = Lu perovskites, as shown in Table 1. This parameter not only increases as a consequence of the octahedral tilting, but it is also a measure of the distortion of the octahedra: both effects are superposed and influence the lattice parameters, together with a more subtle effect due to distortions of the O−V−O angles of the octahedron. The regular evolution of the orthorhombic strain, *s*, with the $R^{3+}$ size is observed in Figure 5. On the other hand, the tilting angle V−O−V of the $VO_6$ octahedra in $RVO_3$ can be obtained from the <V−O−V> bond angle as $\varphi = 180 - <V-O-V>/2$. The variation of $\varphi$ with the $R^{3+}$ size is also plotted in Figure 5. A progressive increase of the tilting angle is observed as the $R^{3+}$ size decreases, from $\varphi = 11.6°$ for R = La to $\varphi = 19.1°$ for R = Lu. This evolution is softer than that observed for the strain parameter, suggesting that the increase in *s* is not only driven by the tilting of the $VO_6$ octahedra.

The variation in V−O distances along the series is represented in Figure 6. Although the average <V−O> values do not significantly evolve with the R size, individual V−O bond lengths significantly diverge for the first terms of the series, from La to Tb. V−O1(medium) and V−O2 (short) distances converge again for the smallest members of the series. The data for Y tend not to follow perfectly the trends for the other R elements, as also observed in Figures 4 and 5. This suggests that a mass effect may be important for Y, as well as the size for R ions. To quantify the relative distortion of the octahedra we define the $\Delta_d$ parameter, concerning the deviation of V−O distances with respect to the average <V−O> value, as $\Delta_d = (1/6)\Sigma_{n=1,6}[(d_n - <d>)/<d>]^2$, see Table 3 and Figure 7. For $LaVO_3$, $\Delta_d$ is very small ($1.9 \times 10^{-7}$), indicating a negligible octahedral distortion; this parameter substantially increases for the former members of the $RVO_3$ series. $\Delta_d$ is maximum for $TbVO_3$ ($0.33 \times 10^{-4}$) and then it decreases for the smaller rare-earth members of the series, as illustrated in Figure 7. In all cases, the distortion parameter is much smaller than those observed in other perovskite series like $RMnO_3$, where the Jahn–Teller character of $Mn^{3+}$ originates a dramatic electronic-driven distortion; for instance, $\Delta_d = 49.7 \times 10^{-4}$ for $DyMnO_3$ at room temperature.[7]

The low-temperature structural phase transformations of some vanadate perovskites have been studied recently by neutron diffraction, namely for $YVO_3$,[30,31] $CeVO_3$,[32] $NdVO_3$,[31] $TbVO_3$,[31] $SmVO_3$,[33] $YbVO_3$,[17] and $LuVO_3$.[34,35] Below a transition temperature $T_{OO1}$, the crystal structure becomes monoclinic $P2_1/n$ because of the establishment of a G-type orbital ordered state: the two valence electrons of the $V^{3+}$ ions occupy alternatingly the $d_{zx}$ and $d_{yz}$ orbitals, with the $d_{xy}$ orbitals always being occupied. For the smallest rare-earths (including Y) there is a second structural transition at $T_{OO2}$ to a third crystallographic structure (again with space group *Pbnm*) exhibiting a different C-type orbital ordering, as recently studied for $YVO_3$.[30,31] The sequence of phase transitions in $RVO_3$ with the size of the $R^{3+}$ ion was studied as a function of temperature from specific heat measurements by Miyasaka et al.,[36] who mapped out the spin–orbital phase diagram of this family of perovskites, showing that $T_{OO1}$ increases from Ce (122 K) to Gd (210 K) and then decreases to 171 K for Lu. It was stated that while in the high-temperature, orbital-disordered phase, the lattice distortions away from the ideal cubic perovskite are determined entirely by ionic-size effects, a strong cooperative Jahn–Teller effect is active in the low temperature phases. In the present study,

(30) Blake, G. R.; Palstra, T. T. M.; Ren, Y.; Nugroho, A. A.; Menovsky, A. A. *Phys. Rev. Lett.* **2001**, *87*, 245501.
(31) Reehuis, M.; Ulrich, C.; Pattison, P.; Ouladdiaf, B.; Rheinstädter, M. C.; Ohl, M.; Regnault, L. P.; Miyasaka, M.; Tokura, Y.; Keimer, B. *Phys. Rev. B* **2006**, *73*, 94440.
(32) Muñoz, A.; Alonso, J. A.; Casais, M. T.; Martínez-Lope, M. J.; Martínez, J. L.; Fernández-Díaz, M. T. *Phys. Rev. B* **2003**, *68*, 144429.
(33) Sage, M. H.; Blake, G. R.; Nieuwenhuis, G. J.; Palstra, T. T. M. *Phys. Rev. Lett.* **2006**, *96*, 36401.
(34) Muñoz, A.; Alonso, J. A.; Casais, M. T.; Martínez-Lope, M. J.; Martínez, J. L.; Fernández-Díaz, M. T. *Chem. Mater.* **2004**, *16*, 1544.
(35) Muñoz, A.; Alonso, J. A.; Casais, M. T.; Martínez-Lope, M. J.; Martínez, J. L.; Fernández-Díaz, M. T. *J. Magn. Magn. Mater.* **2004**, *2163*, 272–276.
(36) (a) Miyasaka, S.; Okimoto, Y.; Iwama, M.; Tokura, Y., *Phys. Rev. B* **2003**, *68*, 100406(R). (b) Brown I. D., *Structure and Bonding in Crystals*; O'Keeffe, M., Navrotsky, A., Eds.; Academic Press: New York, 1981; Vol. 2, pp 1–30..

**Table 3.** Main Bond Distances (Å) and Selected Angles (deg) for Orthorhombic $RVO_3$(R = La, Pr, Nd, Tb, Ho, Er, Tm, Yb, Lu, Y) Perovskites; Determined from NPD at 295 K

| | La | Ce | Pr | Nd | Tb | Y | Ho | Er | Tm | Yb | Lu |
|---|---|---|---|---|---|---|---|---|---|---|---|
| R−O1 | 2.587(3) | 2.527(6) | 2.470(3) | 2.446(3) | 2.331(2) | 2.297(3) | 2.304(4) | 2.284(5) | 2.263(6) | 2.261(2) | 2.256(3) |
| R−O1 | 3.159(4) | 3.147(9) | 3.172(5) | 3.170(3) | 3.177(2) | 3.182(3) | 3.184(4) | 3.177(4) | 3.170(5) | 3.190(2) | 3.188(3) |
| R−O1 | 2.415(4) | 2.403(9) | 2.362(5) | 2.344(3) | 2.272(2) | 2.241(3) | 2.239(4) | 2.234(4) | 2.231(5) | 2.202(2) | 2.192(3) |
| R−O2 ×2 | 2.668(2) | 2.634(6) | 2.639(3) | 2.611(2) | 2.525(2) | 2.495(2) | 2.510(3) | 2.486(3) | 2.507(4) | 2.474(1) | 2.462(2) |
| R−O2 ×2 | 2.776(2) | 2.748(5) | 2.714(2) | 2.709(2) | 2.680(1) | 2.276(2) | 2.669(2) | 2.667(3) | 2.657(3) | 2.665(1) | 2.670(1) |
| R−O2 ×2 | 2.453(2) | 2.405(5) | 2.398(3) | 2.380(2) | 2.302(2) | 2.673(2) | 2.273(3) | 2.271(3) | 2.239(4) | 2.236(1) | 2.227(2) |
| <R−O> 8 short | 2.600(2) | 2.57(2) | 2.542(3) | 2.524(2) | 2.452(2) | 2.428(2) | 2.431(3) | 2.421(3) | 2.413(4) | 2.402(2) | 2.396(2) |
| V−O1 × 2 (s) | 2.0035(6) | 1.9986(9) | 1.9982(5) | 1.9966(1) | 1.9945(6) | 1.9965(7) | 1.9979(9) | 1.996(1) | 1.996(1) | 1.9996(6) | 2.0006(6) |
| V−O2 × 2 (l) | 2.002(2) | 2.009(3) | 2.0116(14) | 2.0148(17) | 2.0227(14) | 2.020(2) | 2.024(2) | 2.018(3) | 2.020(3) | 2.0216(14) | 2.0220(15) |
| V−O2 × 2 (m) | 2.002(2) | 2.004(3) | 2.0082(14) | 2.010(2) | 2.0125(13) | 2.013(2) | 2.011(2) | 2.010(2) | 2.004(3) | 2.0042(13) | 1.9996(14) |
| <V−O> | 2.003(2) | 2.004(2) | 2.006(2) | 2.0089(17) | 2.0099(9) | 2.010(2) | 2.011(2) | 2.008(2) | 2.007(2) | 2.0081(5) | 2.007(1) |
| $10^4\Delta_d$ | 0.0019 | 0.045 | 0.080 | 0.143 | 0.336 | 0.248 | 0.281 | 0.241 | 0.250 | 0.223 | 0.295 |
| V−O1−V | 156.28(3) | 154.92(4) | 153.35(2) | 151.94(3) | 145.69(2) | 143.48(3) | 143.52(4) | 143.16(4) | 142.29(5) | 141.30(2) | 140.75(3) |
| V−O2−V | 157.32(7) | 154.6(1) | 152.57(6) | 151.33(7) | 146.49(5) | 145.03(5) | 145.07(8) | 144.7(1) | 144.1(1) | 143.17(5) | 142.88(6) |
| <V−O−V> | 156.80(5) | 154.76(7) | 152.96(4) | 151.64(5) | 146.09(4) | 144.26(5) | 144.30(6) | 143.93(7) | 143.20(8) | 142.24(4) | 141.82(5) |

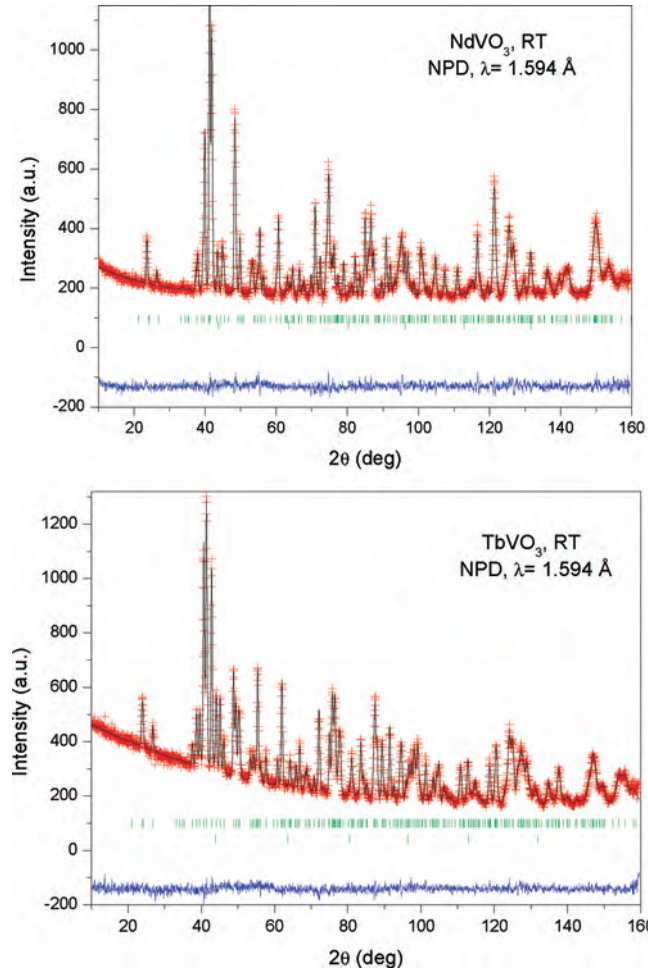


**Figure 3.** Observed (crosses), calculated (full line), and difference (bottom) NPD Rietveld profiles for $NdVO_3$ and $TbVO_3$ ($\lambda = 1.594$ Å). The second series of tick marks correspond to the allowed Bragg reflections for V from the sample holder.

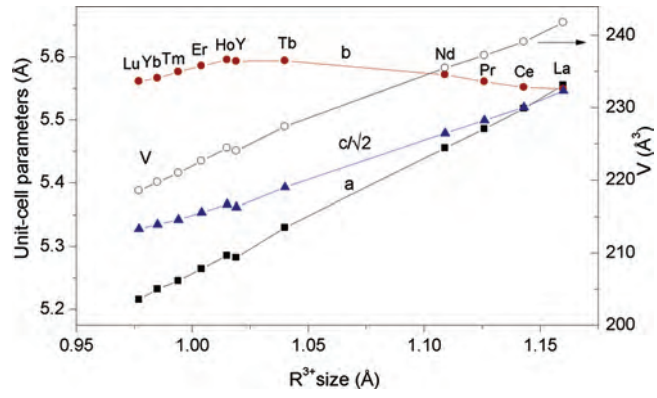


**Figure 4.** Variation of unit-cell parameters and volume with the $R^{3+}$ ionic radii.[29]

carried out at RT, $RVO_3$ perovskites are significantly above the orbital ordering temperature, and thus the electron–lattice coupling is expected to be nonexistent. It would be tempting to explain the observed variation of $\Delta_d$ as simply due to steric effects induced by the tilting of the octahedra as R becomes smaller; however we observe a distinct variation of $\Delta_d$ (Figure 7) than that experienced for the tilting angle or the strain parameter (Figure 5): whereas $\varphi$ or $s$ regularly increase along the series, $\Delta_d$ decreases for the smallest rare earth

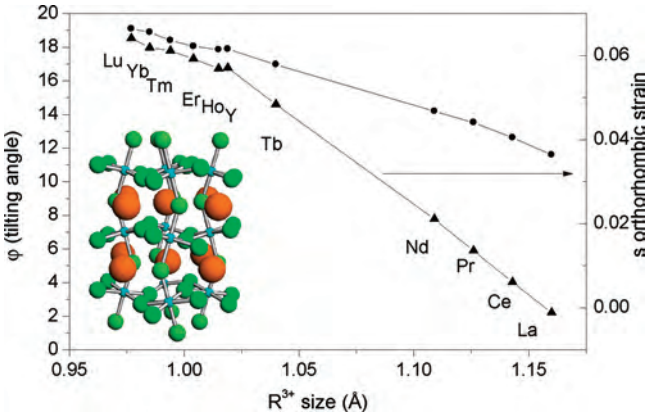


**Figure 5.** Evolution of the average tilting angle ($\varphi$) and the observed strain ($s$) with the $R^{3+}$ ionic radius.[29] The inset shows a view of the orthorhombic *Pbnm* crystal structure (*c*-axis vertical), showing the tilting of $VO_6$ octahedra, with the large R atoms in the voids between them.

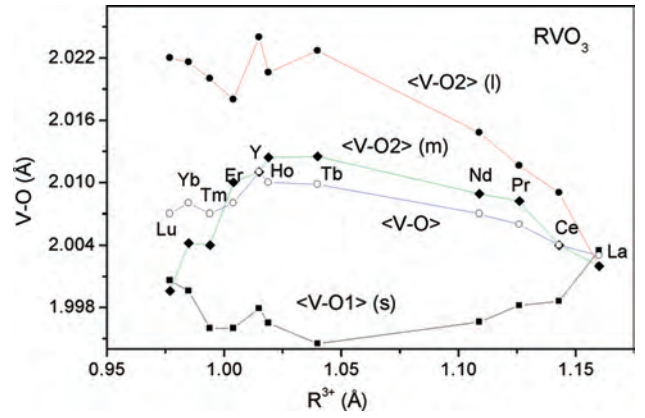


**Figure 6.** Evolution of the V−O bond-lengths along the $RVO_3$ series. *l*, *m*, and *s* stand for long, medium, and short bonds, as defined in Table 3.

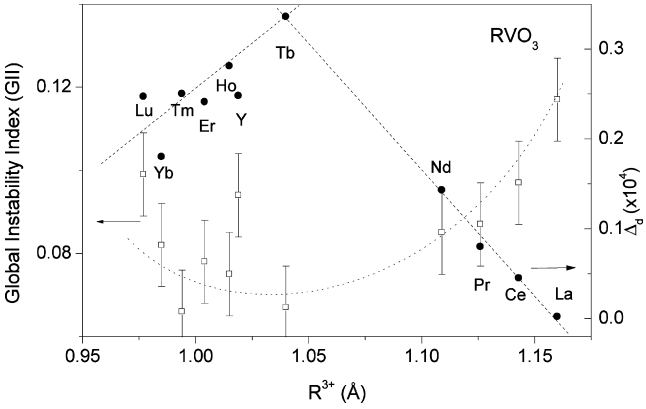


**Figure 7.** Evolution of the $\Delta_d$ distortion parameter of the $VO_6$ octahedra (right axis) and the global instability index (GII) with the $R^{3+}$ ionic size..[29] The dotted and dashed lines are guides for the eye.

cations. Therefore, we suggest the existence of a non-negligible mixing with a nondegenerate state that is more apparent for the $RVO_3$ members with intermediate rare-earths (Tb), which were shown to exhibit the highest $T_{OO1}$ transition temperatures.[36] The fact that the anisotropy of the V−O bonds seems to rapidly increase from La to Tb can be explained by the progressive reduction of the covalent contribution of V−O bonds, which in turn is due to the reduction of the electropositive character from La to Tb. For the smaller rare-earth cations, the establishment of a cooperative orbitally ordered crystal structure is hindered by the increasing distortion of the perovskite through the tilting of the $VO_6$ octahedra, hence reducing the $T_{OO1}$ transition temperature and, at RT, suppressing the electronic contribution to the octahedral distortion and decreasing the $\Delta_d$ parameter to values close to those corresponding to the pure steric contribution. The same boundary for the ionic radius corresponding to Tb is identified for the pressure dependence of ln $T_N$ of the whole family of $RVO_3$ perovskites;[37] the type-G orbital ordering below $T_{OO1}$ enhances the intrinsic octahedral-site distortion and lowers the structure symmetry from *Pbnm* to $P2_1/n$. Therefore, the structural bias is clearly the driving force for the maximum of $T_{OO1}$ for ionic radii between Gd and Tb.

The valence of the cations and anions present in the solid can be estimated by means of the Brown's bond valence model,[38,39] which gives a phenomenological relationship between the formal valence of a bond and the corresponding bond length. In perfect nonstrained structures the bond valence sum (BVS) rule states that the formal charge of the cation (anion) is equal to the sum of the bond valences around this cation (anion). This rule is satisfied only if the stress introduced by the coexistence of different structural units can be relieved by the existence of enough degrees of freedom in the crystallographic structure. The departure of the BVS rule is a measure of the existing stress in the bonds of the structure. The overall stress can be quantified by means of a global instability index (GII),[40] calculated as the root mean of the valence deviations for the $j = 1 \ldots N$ atoms in the asymmetric unit, according to GII $= (\Sigma_j \Sigma_i (s_{ij} - V_j)^2]/N^{1/2}$. Table 4 lists the valences calculated for R, V, and O atoms from the individual R−O and V−O distances of Table 3, as well as GII. Figure 7 plots the variation of GII along the series; the typical error bar for this magnitude is ±0.01. V atoms exhibit valences slightly below but very close to +3, as expected. For the rare-earth cations the valences are also somewhat smaller than +3, which could indicate that R−O are under a slight tensile stress. The GII index is below 0.1 for all the compounds excepting $LaVO_3$ with GII = 0.117. After a slight reduction in GII for the three first members, there is no significant evolution of the GII factor along the series, which suggests that the structural stress induced as $R^{3+}$ becomes smaller is successfully relieved by the tilting and distortion of the octahedral units permitted in the space group *Pbnm*. Actually, crystal structures with GII higher than 0.1 are usually considered as strained, susceptible to experience phase transitions to a more stable polytype as temperature is increased. In fact, high-temperature structural studies on $LaVO_3$ demonstrate that the room-temperature structure has a limited stability range, experiencing a phase transition to a rhombohedral phase at 1113 K, and a further transition to a simple cubic perovskite at 1298 K.[41] To the best of our knowledge, there are no structural studies above

(37) Zhou, J.-S.; Goodenough, J. B.; Yan, J.-Q.; Ren, Y. *Phys. Rev. Lett.* **2007**, *99*, 156401.
(38) Brese, N. E.; O'Keeffe, M. *Acta Crystallogr., Sect. B* **1991**, *47*, 192.
(39) Brown, I. D. *Z. Kristallogr.* **1992**, *199*, 255.
(40) Zubkov, V. G.; Bazuev, G. V.; Shveikin, G. P. *Sov. Phys. Crystallogr.* **1980**, *25*, 103.

**Table 4.** Valence Determined from the Bond Valence Model[a] for R, V, and O at 295 K

| | La | Ce | Pr | Nd | Tb | Y | Ho | Er | Tm | Yb | Lu |
|---|---|---|---|---|---|---|---|---|---|---|---|
| R | 2.793(8) | 2.850(8) | 2.86(1) | 2.865(8) | 2.941(6) | 2.874(7) | 2.93(1) | 2.90(1) | 2.92(1) | 2.897(5) | 2.852(7) |
| V | 2.975(5) | 2.966(6) | 2.947(4) | 2.941(5) | 2.917(4) | 2.919(4) | 2.912(6) | 2.937(7) | 2.944(7) | 2.930(4) | 2.937(4) |
| O1 | 1.931(6) | 1.941(7) | 1.950(8) | 1.960(6) | 2.025(5) | 2.016(6) | 2.030(8) | 2.034(9) | 2.04(1) | 2.032(4) | 2.013(5) |
| O2 | 1.918(5) | 1.916(5) | 1.928(5) | 1.923(5) | 1.917(4) | 1.888(4) | 1.905(6) | 1.902(7) | 1.915(7) | 1.898(3) | 1.888(4) |
| GII | 0.117 | 0.097 | 0.087 | 0.085 | 0.067 | 0.094 | 0.075 | 0.078 | 0.066 | 0.082 | 0.098 |

[a] The valence is the sum of the individual bond valences ($s_i$) for R-O and V-O bonds. Bond valences are calculated as $s_i = \exp[(r_0-r_i)/B]$; $B=0.37$, $r_0=1.743$ for the $V^{3+}-O^{2-}$ pair; for the $R^{3+}-O^{2-}$ pairs, for La, Ce, Pr, Nd, Tb, Y, Ho, Er, Tm, Yb, Lu, $r_0 = 2.172, 2.151, 2.135, 2.117, 2.049, 2.014, 2.023, 2.010, 2.000, 1.985, 1.971$, respectively, from ref. 38. Individual R−O and V−O distances ($r_i$) are taken from Table 3. The global instability index (GII) is calculated as the root mean of the valence deviations for the $j = 1N$ atoms in the asymmetric unit, according to $GII = (\Sigma_j[\Sigma_i(s_{ij}-V_j)^2]/N)^{1/2}$.

RT for the remaining rare-earth vanadates, although from our GII values, we can predict structural stabilities comparable, at least, to that observed for $LaVO_3$.

## Conclusions

As a summary, the members of the $RVO_3$ perovskite family have been studied in the widest range of ionic sizes, reaching the most distorted member $LuVO_3$. A neutron diffraction study at room temperature shows that all the compounds exhibit the same orthorhombically distorted perovskite structure, defined in the Pbnm space group. A simple steric factor accounts for the increase in the global distortion of the perovskite structure, as far as the degree of tilting of the $VO_6$ octahedra is concerned. Additionally, the $VO_6$ octahedra also become progressively distorted, from the virtually undistorted $LaVO_3$ to $TbVO_3$, and then the axial octahedral distortion slightly decreases for last members of the series. Even for $TbVO_3$, the degree of octahedral distortion is 2 orders of magnitude smaller than some strongly Jahn–Teller distorted octahedral units, such as $MnO_6$ in $RMnO_3$ perovskites, were the primary driving factor for distortion is electronic. In $RVO_3$, even if the orbital-ordering temperature described for some members of the series is significantly below room temperature, the distinct evolution of the distortion parameter compared with the strain or tilting angle of the octahedra suggests that the electron–lattice interactions are non negligible and they increase as the covalency of the V−O bonds is reduced along the series, leading to a maximum octahedral distortion for $TbVO_3$.

**Acknowledgment.** We acknowledge the financial support of the Spanish Ministry of Education through Project MAT2007-60536. We thank ILL for making the beamtime available.

IC701969Q